

# Joint OFDM Waveform Design for Communications and Sensing Convergence

Sahan Damith Liyanaarachchi, Carlos Baquero Barneto, Taneli Riihonen, and Mikko Valkama  
Electrical Engineering, Faculty of Information Technology and Communication Sciences, Tampere University, Finland  
email: sahan.liyanaarachchi@tuni.fi

**Abstract**—This paper discusses waveform design for a joint radar and communication system, where the radar transceiver and the communication transmitter are considered to be the same full-duplex base station. The downlink orthogonal frequency-division multiplexing (OFDM) waveform of the communication system is used also for sensing. Thus, unused subcarriers within the OFDM symbols are exploited for radar purposes and filled up with optimized complex-valued data, so as to minimize the lower bounds of the variances of the delay and Doppler estimates of radar target parameters, while maintaining an acceptable level of performance for the communication system. The results indicate that significant improvements can be made for the radar system, but in compensation, the power allocated for the communication subcarriers needs to be reduced. Thus, a trade-off between the converged systems allows both to operate together with reduced performance degradation.

## I. INTRODUCTION

Conventional radar and communication systems operate separately at predefined frequencies so that one does not interfere the other. The ever-increasing demand for mobile communication devices has resulted them being ubiquitous, and to keep up with this demand, spectrum authorities have extended the bands of operational frequencies of these, thereby overlapping on the frequency bands of legacy radar systems, resulting in mutual interference to both systems. Instead of the two systems' separated operation, a joint system thus needs to be devised to mitigate the interference to both systems and allow satisfactory performance, and different solutions have surfaced to address this [1]. Radio-frequency convergence is the most novel category of solutions that encompasses methods where both systems jointly use the available scarce spectrum [2], [3], is also the focus of this paper.

In a joint system with co-located transmitter (TX) antennas for radar and communication systems, a joint waveform is used for both, and it can be differentiated on time, frequency, code and space domains, by having them orthogonal to each other [4]. However, to address the spectrum scarcity evident in the present world, modern systems utilize the same frequency allocation. Thus, in principle, the performance of each system is dependent on the proportion of bandwidth allocated for it, and the improved performance of one happens at the cost of reduced performance of the other [5].

Most often, a joint waveform is generated through an optimization algorithm, while considering the performance of both radar and the communication systems. The function to be optimized is taken as some metric of performance of either

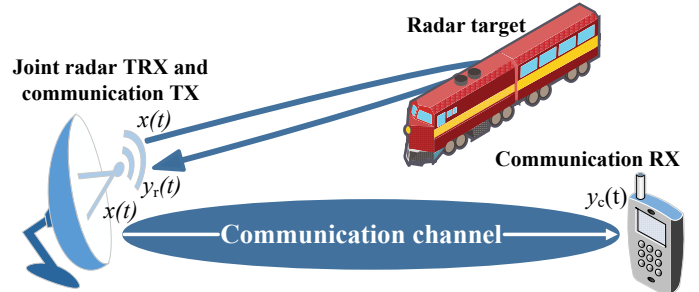


Fig. 1. Joint radar and downlink communication system.

system, while the performance of the other is often set as a constraint. In the perspective of the radar system, performance can be improved by maximizing the signal-to-interference-plus-noise ratio at the radar receiver (RX). The interference on the communication system by the radar system can be controlled by imposing a constraint to reduce the energy in the interfering bands of frequencies [6]. More constraints can also be applied to achieve a better radar waveform, with some properties being the range resolution, modulus of the signal, and integrated and peak side-lobe levels of the autocorrelation function [7]. Another waveform optimization method could be to maximize the detection probability of the radar system while constraining the probability of false alarm. The performance of the communication system can be controlled by imposing a constraint on its capacity [8].

Some researchers have also proposed to maximize the mutual information at the radar RX [9]. A communication system can be used passively here so that the reflected signals from it are also used for target detection. Thus, mutual information about the targets from both radar and communication systems is maximized to generate the waveform [10], [11]. Others have generated the waveform based on target delay estimation, where the Cramer–Rao lower bound (CRLB) of the delay parameter is optimized [12], [13].

This paper concerns the generation of a joint orthogonal frequency-division multiplexing (OFDM) waveform for a converged radar and communication system, as illustrated in Fig. 1. Unlike earlier research on the topic, this paper considers the ability of the base stations of modern OFDM systems to perform also sensing. There often exist unused subcarriers that are not utilized by the communication system, and these can be filled with optimized complex-valued data to improve the

performance of the radar system, based on the minimization of the CRLBs of error variances of the delay and Doppler estimates of the targets, while ascertaining the performance of the communication system is retained at a satisfactory level. The power allocated to the filled *radar subcarriers* and communication subcarriers is set to maintain uniform spectral density, due to which the improved performance of one will come at the expense of the other.

## II. SYSTEM MODEL

Figure 1 depicts the considered joint system architecture. The radar transceiver (TRX) and the communication TX are considered to be the same device, e.g., a base station. Thus, it also receives in full-duplex manner the reflected echoes to perform sensing. The transmit signal  $x(t)$  is an OFDM waveform with  $M$  symbols and each with  $N$  subcarriers. The received signals at the radar RX and the communication RX are denoted by  $y_r(t)$  and  $y_c(t)$ , respectively.

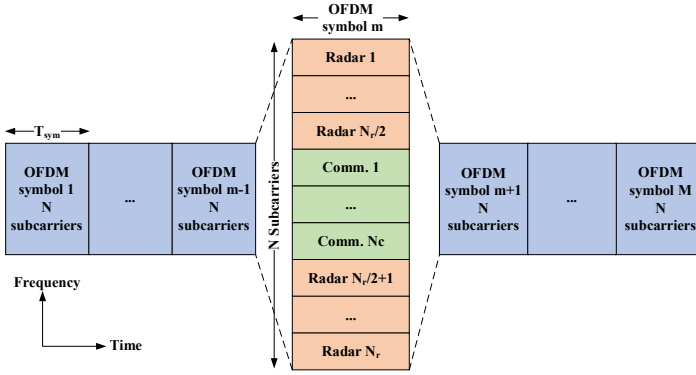


Fig. 2. Structure of the transmitted joint OFDM waveform.

The locations of the radar subcarriers are assumed to be symmetrically placed at the two edges of OFDM spectrum while the communication subcarriers are at the center, as denoted in Fig. 2. Here,  $N_c$  and  $N_r$  are the number of communication and radar subcarriers in an OFDM symbol, respectively, and  $N_c + N_r = N$ . The transmitted complex symbols on a radar and a communication subcarrier are denoted by  $X_{r,n,m}$  and  $X_{c,n,m}$ , where the  $n$  and  $m$  correspond to subcarrier and OFDM symbol indices, respectively.

The radar system performs detection with the help of both radar and communication subcarriers, at the radar RX. For the radar subcarriers, each symbol's amplitude and phase can be freely controlled, whereas for the communication subcarriers, such freedom is not evident. For them, the amplitudes are herein scaled according to the power allocated, prior to optimization, and they are not modified by the optimization.

The joint transmit signal can be written as

$$x(t) = \frac{1}{N} \sum_{m=0}^{M-1} p(t - mT_{\text{sym}}) \left( \sum_{n \in \mathcal{R}} X_{r,n,m} e^{j2\pi n \Delta f (t - mT_{\text{sym}})} + \sum_{n \in \mathcal{C}} X_{c,n,m} e^{j2\pi n \Delta f (t - mT_{\text{sym}})} \right), \quad (1)$$

where  $\Delta f$ ,  $p(t)$ ,  $T_{\text{sym}}$ ,  $\mathcal{C}$  and  $\mathcal{R}$  denote the frequency spacing between subcarriers, the pulse shape, the time duration of an OFDM symbol and sets for communication and radar subcarriers in each OFDM symbol with  $\mathcal{C} = \{n | n \in [\frac{-N_c}{2}, \frac{N_c}{2} - 1]\}$  and  $\mathcal{R} = \{n | n \in [\frac{-N}{2}, \frac{-N}{2} + \frac{N_r}{2} - 1] \cup [\frac{N}{2} - \frac{N_r}{2}, \frac{N}{2} - 1]\}$ . The power of the radar and communication sub-waveforms over  $M$  symbols can then be written as

$$P_r = \frac{1}{MN} \sum_{m=0}^{M-1} \sum_{n \in \mathcal{R}} |X_{r,n,m}|^2, \quad (2a)$$

$$P_c = \frac{1}{MN} \sum_{m=0}^{M-1} \sum_{n \in \mathcal{C}} |X_{c,n,m}|^2. \quad (2b)$$

### A. Radar System

The received radar signal at the radar RX can be written as

$$y_r(t) = \sum_{k=1}^{K_r} A_{r,k} x(t - \tau_{r,k}) e^{j2\pi f_{r,D,k} t} + v_r(t), \quad (3)$$

which is the sum of multiple copies of attenuated and delayed versions of  $x(t)$ . Further, the phases are also varying due to the Doppler shifts, which correspond to the relative speed between the radar TRX and targets. Here,  $K_r$  and  $A_{r,k}$  are the total number of point targets and the two-way attenuation constant for the path between the radar TRX and the  $k^{\text{th}}$  target, while  $\tau_{r,k}$  and  $f_{r,D,k}$  are the two-way delay and Doppler shift of the target, respectively, that the radar tries to estimate. The noise  $v_r(t)$  is assumed to be additive, white, and Gaussian. The signal-to-noise ratio (SNR) at the radar RX due to the  $k^{\text{th}}$  target is

$$\text{SNR}_{r,k} = \frac{|A_{r,k}|^2 P_r}{\sigma_r^2}, \quad (4)$$

where  $\sigma_r^2$  is the variance of the noise samples.

Substituting (1) to (3) and performing the discrete Fourier transform (DFT) yields after simplification the relation between the frequency-domain TX and RX symbols as

$$Y_{r,n,m} = \sum_{k=1}^{K_r} A_{r,k} X_{n,m} e^{-j2\pi n \Delta f \tau_{r,k}} e^{j2\pi f_{r,D,k} m T_{\text{sym}}} + V_{r,n,m}, \quad (5)$$

where  $X_{n,m}$ ,  $Y_{r,n,m}$  and  $V_{r,n,m}$  are the transmitted frequency-domain symbol, received frequency-domain symbol at the radar RX, and the frequency-domain noise sample, all on the  $n^{\text{th}}$  subcarrier and the  $m^{\text{th}}$  OFDM symbol, respectively.

It is observed from (5) that the received noisy frequency-domain symbol has been attenuated and the phase of it has changed from that of the transmitted symbol, due to the delay and Doppler shift of each target. The received frequency-domain symbols can be represented in matrix notation for the case of a single target, assuming the attenuation constant is known, as

$$\mathbf{Y} = \mathbf{D}\mathbf{X}\mathbf{B} + \mathbf{V}, \quad (6)$$

where  $\mathbf{Y}$  is the received symbol matrix of size  $N \times M$  with  $(\mathbf{Y})_{n,m} = Y_{r,n,m}$ ,  $\mathbf{D} = \text{diag}(\mathbf{d})$  is a diagonal matrix of size  $N \times N$  where each element is given by  $\mathbf{d}_n = e^{-j2\pi n \Delta f \tau}$ , and

$n \in \{-N/2, \dots, N/2 - 1\}$ . The transmitted symbol matrix  $\mathbf{X}$  is of size  $N \times M$  with  $(\mathbf{X})_{n,m} = X_{n,m}$ ,  $\mathbf{B} = \text{diag}(\mathbf{b})$  is a diagonal matrix of size  $M \times M$  where each element is given by  $\mathbf{b}_m = e^{j2\pi m f_D T_{\text{sym}}}$ , and  $m \in \{0, \dots, M - 1\}$ . The noise matrix  $\mathbf{V}$  is of size  $N \times M$  with  $(\mathbf{V})_{n,m} = V_{n,m}$ .

### B. Maximum Likelihood Estimation

The radar system uses the received frequency-domain symbols to estimate the delays and Doppler shifts to the different targets. A maximum likelihood estimator (MLE) is used for this. The parameter vector that needs to be estimated is

$$\boldsymbol{\theta} = [\tau, f_D]^T. \quad (7)$$

Since the noise samples are assumed to be independently and identically Gaussian distributed, the simplified log-likelihood function for (6) can be written based on [14] as

$$\mathcal{L}(\mathbf{Y}; \boldsymbol{\theta}) = \Re \left[ \sum_{m=0}^{M-1} \left( \sum_{n=0}^{N-1} Z_{n,m} e^{-j2\pi n \Delta f \tau} \right) e^{j2\pi m f_D T_{\text{sym}}} \right], \quad (8)$$

where  $Z_{n,m} = Y_{n,m}^* X_{n,m}$ . It is seen that the inner and outer sums have close similarity to the definitions of DFT and inverse DFT (IDFT). Therefore, the MLE is found with the help of these by quantizing the delay and Doppler parameters as

$$\tau' = \frac{n'}{N \Delta f}, \quad n' = 0, \dots, N - 1, \quad (9)$$

$$f_D' = \frac{m'}{M T_{\text{sym}}}, \quad m' = 0, \dots, M - 1. \quad (10)$$

Substituting these in (8) results in

$$\mathcal{L}(n', m') = \Re \left[ \underbrace{\sum_{m=0}^{M-1} \left( \sum_{n=0}^{N-1} Z_{n,m} e^{-\frac{j2\pi n n'}{N}} \right)}_{\text{element } m' \text{ in } M\text{-length IDFT}} e^{\frac{j2\pi m m'}{M}} \right]. \quad (11)$$

To find the parameters which correspond to the MLE, the values of  $m'$  and  $n'$  are found as those that maximize the log-likelihood function and denoted as

$$(n_{\max}, m_{\max}) = \arg \max \mathcal{L}(n', m'). \quad (12)$$

Finally, these are substituted in (9) and (10) to estimate the parameter value set

$$\hat{\boldsymbol{\theta}} = [\hat{\tau}, \hat{f}_D]^T = \left[ \frac{n_{\max}}{N \Delta f}, \frac{m_{\max}}{M T_{\text{sym}}} \right]^T. \quad (13)$$

### C. Communication System

The impulse response of the communication channel is

$$h_c(t) = \sum_{k=1}^{K_c} A_{c,k} \delta(t - \tau_{c,k}) e^{j2\pi f_{c,D,k} t}, \quad (14)$$

where  $K_c$ ,  $A_{c,k}$ ,  $f_{c,D,k}$  and  $\tau_{c,k}$  are the total number of scatterers in the communication channel, attenuation constant for the path between the communication TX and RX, Doppler

shift and delay of each scatterer, respectively. The received frequency-domain symbols at the communication RX can be written based on (5) as

$$Y_{c,n,m} = \sum_{k=1}^{K_c} A_{c,k} X_{c,n,m} e^{-j2\pi n \Delta f \tau_{c,k}} e^{j2\pi f_{c,D,k} m T_{\text{sym}}} + V_{c,n,m}, \quad (15)$$

where  $Y_{c,n,m}$  and  $V_{c,n,m}$  are received frequency-domain communication symbols and the noise samples, respectively. The SNR of a communication subcarrier can then be denoted as

$$\text{SNR}_{c,n,m} = \frac{\mathbb{E}\{|X_{c,n,m}|^2\} |H_{c,n,m}|^2}{\sigma_c^2}, \quad (16)$$

where  $\mathbb{E}$  and  $\sigma_c^2$  denote the expectation operation and the variance of noise at the communication RX, respectively, and

$$H_{c,n,m} = \sum_{k=1}^{K_c} A_{c,k} e^{-j2\pi n \Delta f \tau_{c,k}} e^{j2\pi f_{c,D,k} m T_{\text{sym}}} \quad (17)$$

is the frequency-domain per-subcarrier representation of the impulse response given in (14). Since the communication RX is assumed to have knowledge about the locations of the radar subcarriers in different OFDM symbols, as is the case with conventional OFDM processing, it can easily discard those, without any extra burden.

### III. OPTIMIZATION OF RADAR SUBCARRIERS

In estimating the parameters according to (11)–(13), they usually deviate from the actual values. It is essential that the variances of these errors be minimized to improve the accuracy of the parameter estimation process. These variances are bounded from below by the CRLBs as [15]

$$\text{var}(\hat{\tau}) \geq \text{CRLB}(\hat{\tau}), \quad (18a)$$

$$\text{var}(\hat{f}_D) \geq \text{CRLB}(\hat{f}_D). \quad (18b)$$

For the signal model in (6), these are given in the Appendix by (27a) and (27b).

The waveform optimization which minimizes the CRLBs of the delay and Doppler estimates can then be denoted as

$$\arg \min_{\mathbf{X}} \text{CRLB}(\hat{\tau}) \text{ or } \arg \min_{\mathbf{X}} \text{CRLB}(\hat{f}_D) \quad (19a)$$

subject to the constraints

$$P_r = \left( \frac{N_r}{N} \right) P_{\text{total}}, \quad (19b)$$

$$\text{PAPR}_{x(t)} \leq \text{PAPR}_{\max}, \quad (19c)$$

where  $\mathbf{X}_r$ ,  $P_{\text{total}}$ ,  $\text{PAPR}_{x(t)}$  and  $\text{PAPR}_{\max}$  denote the matrix of optimized complex-valued data for the radar subcarriers, total TX power, peak-to-average power ratio (PAPR) of the joint waveform and the maximum PAPR tolerable by the TX, respectively. The power between radar and communication subcarriers is dependent on their subcarrier ratio within an OFDM symbol. The first constraint therefore ensures that the radar subcarriers would have a proportion of the total transmit power while the second constraint limits the PAPR of the generated OFDM waveform. In what follows, this optimization problem is numerically solved through the constrained optimization function *fmincon* in MATLAB.

#### IV. NUMERICAL RESULTS

The parameters used for the waveform optimization are  $P_{\text{total}} = 39\text{dBm}$ ,  $\text{PAPR}_{\text{max}} = 8\text{dB}$ ,  $M = 64$ ,  $N = 128$ ,  $\Delta f = 120\text{kHz}$  and carrier frequency  $f_c = 28\text{GHz}$ . Figure 3 depicts the effect of optimization on the root CRLBs for distance and velocity estimates, after converting the delay and Doppler estimates as  $\hat{d} = \frac{c\hat{\tau}}{2}$  and  $\hat{v} = \frac{c\hat{f}_D}{2f_c}$ , with  $c$  being the speed of light. It can be observed that waveform optimization allows reduced root CRLBs when compared with the respective unoptimized waveforms. In the unoptimized cases, the radar subcarriers are assumed to be empty, mimicking the unused subcarriers. The worst errors under optimization for both cases are when all are communication subcarriers. However, the availability of increased number of radar subcarriers allows to further minimize the errors of the radar system. From (19b), it is however evident that the increase of the number of radar subcarriers will imply reduced power for the communication subcarriers.

The waveform optimizations based on the minimization of delay and Doppler estimates' CRLBs are considered as separate optimizations that output two different waveforms, and Fig. 3 also denotes how one waveform optimization affects the other. Due to one waveform optimization, the error of the other estimate also increases with  $N_c$ . However, this is higher than in the case when that particular parameter is the objective for waveform optimization. Thus, the optimization of one impacts in an inverse way on the other, as is the case usually for contrasting optimizations.

Figure 4 shows the PAPR of the waveform for the two optimizations, with and without the PAPR constraint applied. In optimizing the waveform to minimize the CRLB of the distance estimate, it is observed that the PAPR is high when only radar subcarriers exist, and the inclusion of communication subcarriers is seen to decrease the PAPR of the waveform. However, these PAPR values are still considered to be high for the communication system. For the other waveform optimization, though a higher PAPR is not observed w.r.t. the distance case, it is still undesirable for a practical TX. For both of these, it is observed that the addition of the PAPR constraint allows to control the PAPR of the waveform to the required level of 8dB. One point to note is that when all the subcarriers are used for communication, the optimization does not have any degrees of freedom and, thus, the PAPR of the waveform cannot be controlled.

To evaluate the effect on the communication system, a multipath channel is simulated with a free space path loss of 116dB, a noise power of  $-96\text{dBm}$  at the communication RX, root mean square delay spread of 0.63ns and a ratio of  $-13\text{dB}$  between the direct and average multipath components. Each communication symbol  $X_{c,n,m}$  uses quadrature phase-shift keying in this paper. For different channel realizations, the average SNR of the communication subcarriers at the communication RX is calculated and Fig. 5 depicts the variation of the empirical cumulative distribution functions (CDF) for different number of communication subcarriers in each OFDM

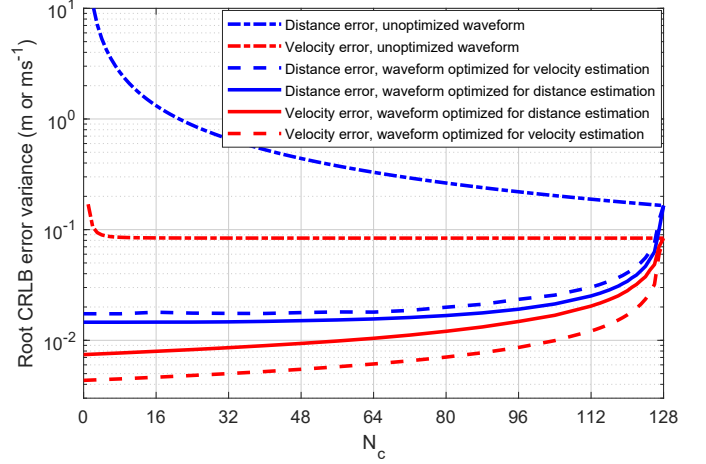


Fig. 3. Root CRLB error variances of the distance and velocity estimates, for optimized and unoptimized waveforms, with  $\text{PAPR}_{\text{max}} = 8\text{dB}$ .

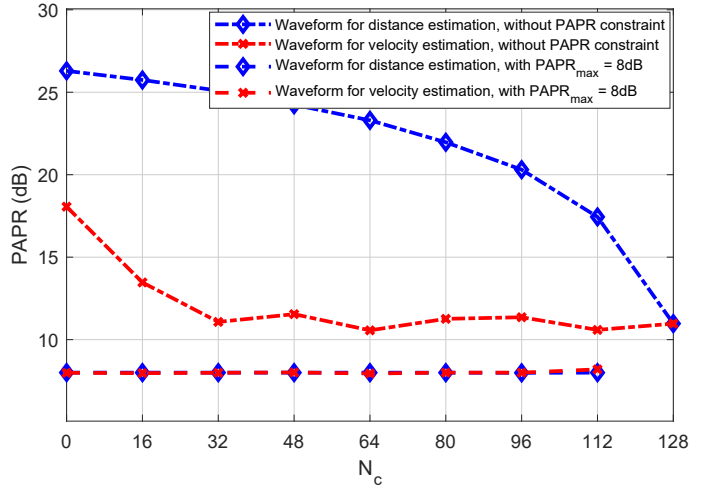


Fig. 4. The effect of constraining the PAPR of the optimized waveforms for distance and velocity estimations, with  $\text{PAPR}_{\text{max}} = 8\text{dB}$ .

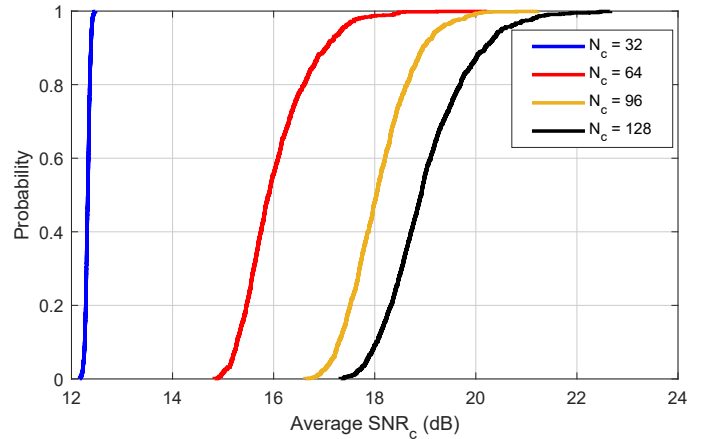


Fig. 5. Empirical CDFs of the average SNR of the communication subcarriers at the communication RX for different number of communication subcarriers, with  $P_{\text{total}} = 39\text{dBm}$ , noise power of  $-96\text{dBm}$ , and free space path loss of 116dB.

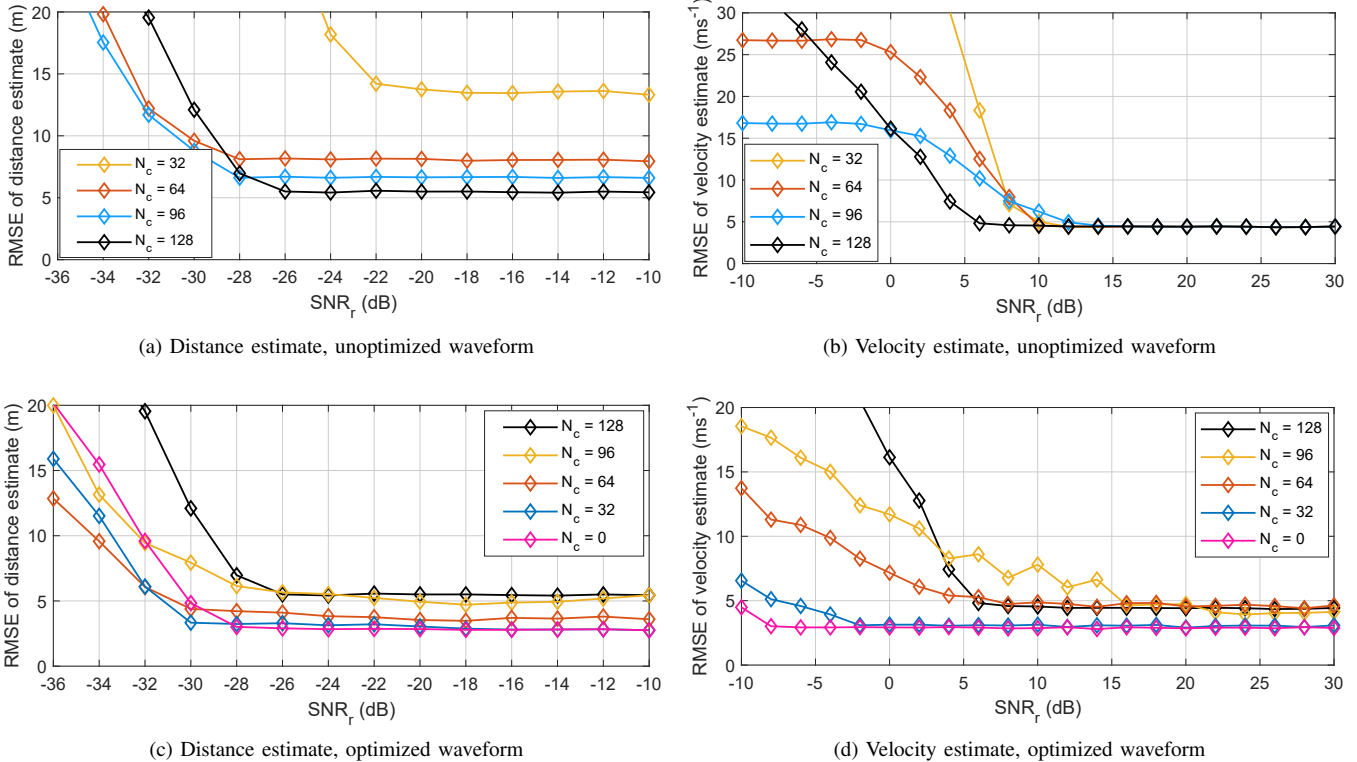


Fig. 6. The RMSE of distance and velocity estimates for the unoptimized and optimized cases, for different number of communication subcarriers.

symbol, where the rest is considered to be filled by the radar subcarriers. Due to this, a part of the total transmit power is allocated for the radar subcarriers, which in turn reduces the power allocated for the communication subcarriers, thus reducing the SNR of the communication subcarriers at the RX. This effect can be observed from the figure in which decreasing the number of communication subcarriers is seen to decrease the average SNR of these subcarriers. This loss of average SNR due to the addition of radar subcarriers is proportional to the ratio of how loaded the OFDM waveform is w.r.t. the communication subcarriers, on average.

Finally, to evaluate the performance of the optimized waveforms for distance and velocity estimation, MLE is performed for a practical scenario. For a range of SNR values at the radar RX, a target with some velocity is placed at some distance, with them being uniformly distributed with standard deviations of the target location and velocity as  $\Delta r = \frac{c}{2N\Delta f}$  [m] and  $\Delta v = \frac{c}{2Mf_c T_{\text{sym}}}$  [ms<sup>-1</sup>]. For each SNR, root mean square error (RMSE) is calculated.

Figure 6 depicts the error performance for unoptimized and optimized waveforms. Figures 6(a) and 6(b) show the effect of the addition of the communication subcarriers for the distance and velocity estimates, for the unoptimized cases, where the rest is considered to be unused. For the distance estimate, increase in the number of communication subcarriers decreases the error, where different error floors are reached, with higher the number of communication subcarriers, lower

the error floor. For the velocity estimate, the same error floor is reached. Figures 6(c) and 6(d) show the effect of optimization through the addition of the radar subcarriers, by decreasing the number of communication subcarriers. For the distance estimate, increase of the number of radar subcarriers allows for reduced errors, while similar performance is observed for the velocity estimate.

## V. CONCLUSION

This paper discussed OFDM waveform design for joint communications and sensing. Unused subcarriers within the radio frames of modern cellular systems employing OFDM are exploited to improve the performance of the radar system, while keeping the performance of the communication system at an acceptable level. The unused subcarriers are filled with optimized complex-valued data through the minimization of the theoretical lower bounds of the parameters of interest of the radar system, namely the delay and Doppler estimates. The results showcase that these bounds can be lowered by waveform optimization at the cost of reducing the power allocated for the communication subcarriers. Thus, the performance improvement of one system is subject to a trade-off with the performance of the other. However, this allows both to work together with reduced performance degradation. Further, the optimized waveforms were shown to offer good performance in actual maximum likelihood estimation. In future work, we extend this to 5G New Radio waveforms and analyze its effects.

## APPENDIX

Converting the matrix notation in (6) to a vectorized form yields

$$\mathbf{y} = \mathbf{s} + \mathbf{v}, \quad (20)$$

where  $\mathbf{y} = \text{vec}(\mathbf{Y})$ ,  $\mathbf{s} = \text{vec}(\mathbf{DXB})$  and  $\mathbf{v} = \text{vec}(\mathbf{V})$  are all of the size  $NM \times 1$ . The mean vector and covariance matrix of  $\mathbf{y}$  can be denoted as

$$\mathbf{m}_y = \mathbf{s}, \quad (21)$$

$$\Sigma = \mathbb{E}(\mathbf{ss}^H) + \sigma^2 \mathbf{I} = \mathbf{ss}^H + \sigma^2 \mathbf{I}, \quad (22)$$

where  $\mathbf{I}$  is an identity matrix of size  $NM \times NM$ . For a given parameter set, the minimum variance of an estimator is given by the CRLB. For the signal model given by (20), CRLBs for the estimators are calculated from [15]

$$I(\theta)_{i,j} = 2\Re \left[ \frac{\partial \mathbf{s}^H}{\partial \theta_i} \Sigma^{-1} \frac{\partial \mathbf{s}}{\partial \theta_j} \right], \quad (23)$$

where  $I(\theta)_{i,j}$  denotes each element of the Fisher information matrix while  $i = 1, 2$  and  $j = 1, 2$  with  $\theta_1 = \tau$  and  $\theta_2 = f_D$ , similar to (7). Depending on the variable with respect to which the vector  $\mathbf{s}$  is differentiated, this can be simplified after substituting for  $\Sigma$  from (22) as

$$I(\theta)_{i,j} = 2\Re \left[ \mathbf{s}^H \mathbf{D}_i (\mathbf{ss}^H + \sigma^2 \mathbf{I})^{-1} \mathbf{D}_j \mathbf{s} \right]. \quad (24)$$

If the differentiating variable is  $\tau$ ,  $\mathbf{D}_i = \mathbf{D}_\tau = \text{diag}(\mathbf{d}_\tau)$ , in which  $\mathbf{d}_\tau$  is a vector of size  $NM \times 1$  where the first  $N$  elements are  $(-N/2, \dots, N/2-1)$  and these  $N$  elements being repeated for  $M$  times. Similarly, if the differentiating variable is  $f_D$ ,  $\mathbf{D}_j = \mathbf{D}_{f_D} = \text{diag}(\mathbf{d}_{f_D})$ , in which  $\mathbf{d}_{f_D}$  is a vector of size  $NM \times 1$  where sets of  $N$  elements are the same, with the starting and ending indices being zero and  $M-1$ , respectively. Each element of the Fisher matrix, which is now of size  $2 \times 2$ , is derived using (24) as

$$I(\theta)_{1,1} = 2\Re \left[ (2\pi \Delta f)^2 \mathbf{s}^H \mathbf{D}_\tau (\mathbf{ss}^H + \sigma^2 \mathbf{I})^{-1} \mathbf{D}_\tau \mathbf{s} \right], \quad (25a)$$

$$I(\theta)_{1,2} = 2\Re \left[ (-4\pi^2 \Delta f T_{\text{sym}}) \mathbf{s}^H \mathbf{D}_\tau (\mathbf{ss}^H + \sigma^2 \mathbf{I})^{-1} \mathbf{D}_{f_D} \mathbf{s} \right], \quad (25b)$$

$$I(\theta)_{2,1} = 2\Re \left[ (-4\pi^2 \Delta f T_{\text{sym}}) \mathbf{s}^H \mathbf{D}_{f_D} (\mathbf{ss}^H + \sigma^2 \mathbf{I})^{-1} \mathbf{D}_\tau \mathbf{s} \right], \quad (25c)$$

$$I(\theta)_{2,2} = 2\Re \left[ (2\pi T_{\text{sym}})^2 \mathbf{s}^H \mathbf{D}_{f_D} (\mathbf{ss}^H + \sigma^2 \mathbf{I})^{-1} \mathbf{D}_{f_D} \mathbf{s} \right]. \quad (25d)$$

Therefore, the Fisher matrix and its inverse are given by

$$I(\theta) = \begin{bmatrix} I(\theta)_{1,1} & I(\theta)_{1,2} \\ I(\theta)_{2,1} & I(\theta)_{2,2} \end{bmatrix}, \quad (26a)$$

$$I^{-1}(\theta) = \frac{\begin{bmatrix} I(\theta)_{2,2} & -I(\theta)_{1,2} \\ -I(\theta)_{2,1} & I(\theta)_{1,1} \end{bmatrix}}{\det I(\theta)}. \quad (26b)$$

Finally, the CRLBs for the two estimators are given by the diagonal elements of the inverse Fisher matrix, where the first diagonal element corresponds to CRLB of the delay estimate

while the second corresponds to that of the Doppler estimate. Thus, these are given as

$$\text{CRLB}(\hat{\tau}) = \frac{I(\theta)_{2,2}}{\det I(\theta)}, \quad (27a)$$

$$\text{CRLB}(\hat{f}_D) = \frac{I(\theta)_{1,1}}{\det I(\theta)}. \quad (27b)$$

## ACKNOWLEDGMENT

This research was partially supported by the Academy of Finland (grants #310991, #315858, and #328214), Nokia Bell Labs, and the Doctoral School of Tampere University. This research was also supported by the Finnish Funding Agency for Innovation through the ‘‘RF Convergence’’ project.

## REFERENCES

- [1] Y. Han, E. Ekici, H. Kremo, and O. Altintas, ‘‘Spectrum sharing methods for the coexistence of multiple RF systems: A survey,’’ *Ad Hoc Networks*, vol. 53, Sep. 2016.
- [2] B. Paul, A. R. Chiriyath, and D. W. Bliss, ‘‘Survey of RF communications and sensing convergence research,’’ *IEEE Access*, vol. 5, pp. 252–270, 2017.
- [3] C. Baquero Barneto, T. Riihonen, M. Turunen, L. Anttila, M. Fleischer, K. Stadius, J. Ryynänen, and M. Valkama, ‘‘Full-duplex OFDM radar with LTE and 5G NR waveforms: Challenges, solutions, and measurements,’’ *IEEE Transactions on Microwave Theory and Techniques*, vol. 67, no. 10, pp. 4042–4054, Oct. 2019.
- [4] Y. Liu, G. Liao, Z. Yang, and J. Xu, ‘‘Design of integrated radar and communication system based on MIMO-OFDM waveform,’’ *Journal of Systems Engineering and Electronics*, vol. 28, no. 4, pp. 669–680, Aug. 2017.
- [5] H. Safavi-Naeini, S. Roy, and S. Ashrafi, ‘‘Spectrum sharing of radar and Wi-Fi networks: The sensing/throughput tradeoff,’’ *IEEE Transactions on Cognitive Communications and Networking*, vol. 1, no. 4, pp. 372–382, Dec. 2015.
- [6] A. Aubry, A. D. Maio, Y. Huang, M. Piezzo, and A. Farina, ‘‘A new radar waveform design algorithm with improved feasibility for spectral coexistence,’’ *IEEE Transactions on Aerospace and Electronic Systems*, vol. 51, no. 2, pp. 1029–1038, Apr. 2015.
- [7] T. Guo and R. Qiu, ‘‘OFDM waveform design compromising spectral nulling, side-lobe suppression and range resolution,’’ in *Proc. IEEE Radar Conference*, May 2014, pp. 1424–1429.
- [8] M. Bica, K. Huang, U. Mitra, and V. Koivunen, ‘‘Opportunistic radar waveform design in joint radar and cellular communication systems,’’ in *Proc. IEEE Global Communications Conference*, Dec. 2015, pp. 1–7.
- [9] M. R. Bell, ‘‘Information theory and radar waveform design,’’ *IEEE Transactions on Information Theory*, vol. 39, no. 5, pp. 1578–1597, Sep. 1993.
- [10] M. Bica, K. Huang, V. Koivunen, and U. Mitra, ‘‘Mutual information based radar waveform design for joint radar and cellular communication systems,’’ in *Proc. IEEE International Conference on Acoustics, Speech and Signal Processing*, Mar. 2016, pp. 3671–3675.
- [11] K.-W. Huang, M. Bica, U. Mitra, and V. Koivunen, ‘‘Radar waveform design in spectrum sharing environment: Coexistence and cognition,’’ in *Proc. IEEE Radar Conference*, May 2015, pp. 1698–1703.
- [12] M. Bica and V. Koivunen, ‘‘Delay estimation method for coexisting radar and wireless communication systems,’’ in *Proc. IEEE Radar Conference*, May 2017, pp. 1557–1561.
- [13] —, ‘‘Radar waveform optimization for target parameter estimation in cooperative radar-communications systems,’’ *IEEE Transactions on Aerospace and Electronic Systems*, vol. 55, no. 5, pp. 2314–2326, Oct. 2019.
- [14] M. Braun, C. Sturm, and F. K. Jondral, ‘‘Maximum likelihood speed and distance estimation for OFDM radar,’’ in *Proc. IEEE Radar Conference*, May 2010, pp. 256–261.
- [15] S. Kay, *Fundamentals of Statistical Signal Processing: Detection theory*. PTR Prentice-Hall, 1993.